Deciphering the microscopic phenomenon behind contact resistances in interlayer functionalized electrodes and organic semiconductors

Kalyani Patrikar* and Anirban Mondal†
Department of Chemistry, Indian Institute of Technology Gandhinagar, Palaj 382355, India

(Received 18 February 2024; revised 7 May 2024; accepted 9 May 2024; published 21 May 2024)

Interlayers are known to enhance the performance of organic devices by reducing contact resistance, however, the details of the mechanism are uncertain. Models have correlated properties of interlayers to their extent of reduction of contact resistance, but a universal parameter correlating the microscopic phenomenon to device characteristics is yet to be established. Here, we demonstrate that the energy-level modulation at the interface of interlayer functionalized electrode and organic semiconductor, combined with the charge transfer integral between them, determines the extent of the reduction of contact resistance. Moreover, the rate of charge transfer calculated from these quantities is demonstrated to be a universal parameter predicting the characteristics of devices with functionalized electrodes, regardless of the nature of the semiconductor (*p*- or *n*-type). These observations explain the mechanism of interlayers and provide a computational model capable of selecting interlayers leading to high-performing devices.

DOI: 10.1103/PhysRevMaterials.8.054606

I. INTRODUCTION

Optoelectronic devices that employ organic semiconductors (OSC) as an active layer, such as in organic light-emitting devices, organic solar cells, or organic field-effect transistors (OFET), have lead to the development of several flexible, conformable, and lightweight systems [1–3]. Organic devices comprise *p*-type or *n*-type OSC, depending on whether the active layer is more efficient in transporting holes or electrons [4–6]. As OSC's intrinsic charge carrier density is low, the devices rely on photogenerated or injected charge carriers for operation. Charge carrier injection is carried out from the device electrodes by injecting electrons to *n*-type OSC or accepting electrons from *p*-type OSC thereby injecting holes. The injection characteristics are considered to be chiefly dependent on the work function of the electrode, as the electron (hole) injection is more feasible from electrodes of low (high) work function [7,8]. However, due to the complex interactions of inorganic and organic materials, interface formation between the electrode and OSC is accompanied by a realignment of the energy levels that setup an energy barrier to charge injection [9,10]. These include pillow effects, image charges, and induced interfacial density of states. Due to these, the final energy levels, and hence the energy barrier, cannot be predicted based on the individual energy levels of OSC and electrodes [11,12]. The consequent resistance at the interface is known as contact resistance (R_C), which acts in series to the resistance of the OSC, thereby hindering the device current and increasing the operating voltage [13].

Suitable interlayers have been known to reduce R_C by modulating the interface so that the energy barrier to injection is lowered [14–17]. However, the mechanism of interlayers at contact interfaces in organic devices still needs to be established. The reduction in R_C has been attributed to the shift in the work function of the electrode surface or alterations in energy-level alignment brought about by the interlayer [18]. Efficient interlayers are considered to modulate the energy levels such that the magnitude of the interface barrier is reduced. It has been shown that physical properties such as the polarity of the interlayer, work function shift of the electrode surface, and orbital interactions at the interface play a crucial role in the reduction of R_C by an interlayer [19–21]. Further, interlayers are known to reduce the effects of image charges and broaden the density of states at the interface [22,23]. However, a general mechanism correlating the microscopic phenomenon related to charge injection with device performance has not been developed. Thorough models that encompass all effects contributing to contact resistance have not been developed. Such a model would be based on microscopic interface processes determined by molecular-scale interactions, which govern the interface properties, and hence, charge transfer. The lack of a universal model correlating molecular properties with device behavior and establishing guidelines for screening interlayer materials has hindered the widespread use of interlayers to enhance the performance of organic devices.

First-principles computations have been carried out to explore the factors determining the reduction of R_C by functionalized interfaces. Studies showed that the dipole and orientation of molecules comprising the interlayer determined its contribution in reducing R_C, as well as properties such as length and orbital positions [24–29]. We showed previously that electronic coupling at the interface, in the form of the charge transfer integral among frontier orbitals, along with interface polarity, decides the extent of R_C reduction by the interlayer [30]. However, *ab intio* computations capturing the factors essential to the charge injection process have not been performed. Density functional theory (DFT)-based

*kalyani.p@iitgn.ac.in
†amondal@iitgn.ac.in

calculations were previously used to simulate interfaces of organic molecules with inorganic films [31]. The projector operator diabatic (POD) method based on DFT was developed to simulate the effects of interface interactions on the physical properties of its components [32,33]. POD calculations have enabled the understanding of the effect of these properties on charge transfer across interfaces [34].

In this work, we simulate the interface of an interlayer functionalized electrode (IFE) with OSC to study the process of charge injection from IFE to OSC. Electron injection to *n*-type OSC and hole injection to *p*-type OSCs are considered. The results of simulation are compared with measured R_C and mobility of organic field effect transistors (OFET) with Au electrodes functionalized with different molecules forming a self-assembled monolayer (SAM) as reported by the authors of Ref. [35]. The factors determining the charge transfer process at the interface are identified, and the corresponding quantities are computed. The energy levels of the entities comprising the interface and parameters representing their electronic coupling were computed. Based on these computed parameters, the charge injection rate was calculated per the Marcus-Hush equation [36,37] and correlated with device R_C. We show that the relative energetic positions of the orbitals and states participating in charge injection and the extent of their interactions as computed by the values of the charge transfer integral determine the charge injection and are correlated with contact resistance. We show that a function of these parameters comprehensively captures the effects of microscopic parameters on device behavior. Here, the function is represented by the charge transfer rate calculated as per the Marcus-Hush equation. The rate thus calculated is presented as a universal parameter determining the extent of the reduction of resistance by an interlayer in organic devices, regardless of the type or structure of the OSC. The comprehensive computational model developed here both provides insight into the mechanisms underlying charge injection in organic systems and provides a parameter for evaluating interlayer performance for a device with universal applicability.

II. METHODS

Electronic structure calculations were based on density functional theory [38,39]. Stacks were setup with the interlayer functionalized electrode (IFE) represented by molecules forming a self-assembled monolayer (SAM) bonded to a slab of Au (the electrode was simulated as four-layered slabs), while an organic semiconductor (OSC) molecule was placed on top. The configuration of the entire stack was optimized; the last two layers of Au were held frozen while the remaining atoms were allowed to be moved. Freezing the last two layers allowed it to represent the bulk of the electrode, which did not interact with the interlayer; meanwhile, the mobile surface layers were free to interact with SAM and OSC molecules. The simulation stack and DFT parameters were based on Ref. [32]. Calculations were carried out using the QUICKSTEP module provided by the CP2K program [40,41]. Geometry optimization was performed by applying the threshold conditions on the gradient of the electronic wave functions and the force on the nuclei with convergence criteria of 10^{-7} and 10^{-2} a.u., respectively. This was followed by calculations based on the POD method, with the OSC molecule defined as a single block and the IFE as another block. Exchange-correlation potentials were treated within the generalized gradient approximation (GGA) employing the Perdew-Burke-Ernzerhof (PBE) functional [42]. The energy cutoff was set to 415 Ry for the auxiliary plane wave expansion of the charge density. Valence electrons were modeled explicitly, whereas core electrons were treated with norm-conserving Goedecker-Teter-Hutter (GTH) pseudopotentials [43,44]. The basis set TZ-GTH was employed for calculating systems with an Au electrode, as it has been well optimized for organic-Au systems [43,44]. For the remaining elements, a triple-ζ valence plus polarization (TZVP) basis set was adopted to expand the wave functions [45,46]. A Fermi-Dirac distribution smearing with electronic temperature 298.15 K was employed, involving metal surface calculations to preserve the fractional occupation of states near the Fermi energy. Properties of the blocks, such as energy levels and the electronic coupling among all states of donor and acceptor, were obtained by invoking the ET_COUPLING module in the PROPERTIES section of CP2K, resulting in the energy level diagram of donor, acceptor, and complex, as well as the electronic coupling between orbitals of donor and states of the acceptor. The reorganization energy was calculated by the four-point method [47]. For each OSC, the ground-state geometry of neutral and charged monomers was optimized, followed by energy calculations for charged and neutral monomers in neutral and charged geometry, respectively. Separate calculations were performed using the package GAUSSIAN09 [48], with HF using a basis set 6-31G(d,p) [49–53].

III. RESULTS

A slice of the OFET contact interface was simulated as a stack consisting of a slab of Au electrode, a molecule of the interlayer SAM, and an OSC molecule as shown in Fig. S1 of the Supplemental Material (SM) [54]. The IFE consists of a SAM molecule bonded via the thiol group to the Au surface. The OSC molecule was positioned on top of IFE, and the complete stack was optimized for each IFE-OSC system. We previously showed this stack to be a computationally efficient yet methodically sufficient configuration to represent the contact interface in the measured device [30]. We deliberately chose systems to study for which we obtained contact resistance values from a single source. Various interlayers employed in Ref. [35] were simulated with the SAM of molecules whose structures and names are given in Fig. 1. Several aliphatic as well as aromatic molecules with diverse functional groups are included. The *n*-type OSC known as N1400, and *p*-type OSC TIPS-pentacene, as well as TFB, were considered, as the R_C of their respective OFETs were reported by Boudinet *et al.* [35]. While N1400 and TIPS-pentacene are molecular semiconductors, TFB is a polymer. The details of the fabrication and measurement of the OFETs are given in Ref. [35]. Molecular structures of all OSCs are displayed in Fig. 1. Stacks with N1400 will be henceforth referred to by the prefix *n*, with TFB as *f*, and with TIPS-pentacene as *t*. The name of the SAM molecule will follow the prefix; e.g., the stack with Au functionalized by the MeTP interlayer and with N1400 as OSC will be referred to as *n*-MeTP. The stack was optimized

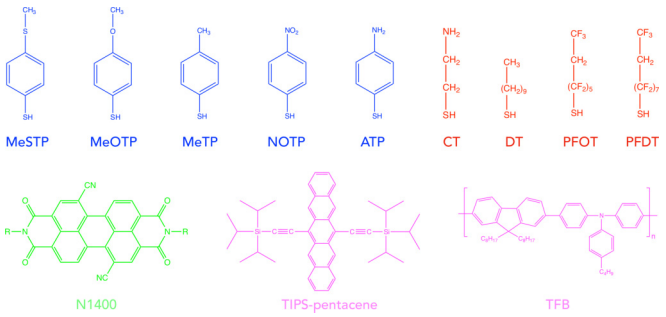

FIG. 1. Schematic of molecular structures of interlayers simulated here, in the form of aromatic or aliphatic self-assembled monolayers, as well as of semiconductors *n*-type N1400, and *p*-type TIPS pentacene and TFB.

using DFT-based methods. Calculations based on the POD method were performed, which allowed the stack to be segregated into donor and acceptor; here, they are IFE and OSC. Values of the respective density of states and energy levels of IFE and OSC were obtained, and the charge transfer integral between states on IFE and orbitals of OSC participating in charge transport was computed. Based on these values, the charge transfer rate across the interface was calculated per the Marcus-Hush equation. As charge injection depends on the energy levels and occupation of electrons, the density of states on IFE and OSC were computed. Energy levels available on IFE and OSC were calculated by first principles by employing the POD method. Figure 2 shows the energy levels at which states are available on either IFE or OSC. A particular energy level on IFE may have *n*-degenerate states. Figures 2(a) to 2(c) correspond to stacks with N1400 and IFE with interlayers as Fig. 2(a) PFDT (*n*-PFDT), Fig. 2(b) CT (*n*-CT), and Fig. 2(c) MeTP (*n*-MeTP). These stacks correspond to the highest, medium, and lowest R_C for the respective OFETs. Energy-level diagrams for the remaining stacks with N1400 are shown in Fig. S2 of the SM. Similarly, Figs. 2(d) to 2(f) exhibit a density of states for stacks with TFB, with interlayers in Fig. 2(d) MeOTP (f-MeOTP), Fig. 2(e) ATP (f-ATP), and Fig. 2(f) PFOT (f-PFOT), corresponding to the highest, medium, and lowest R_C for the respective OFETs. The energy-level diagrams for the remaining stacks with TFB are displayed in Fig. S3 of the SM. Further, Figures 2(g) to 2(i) exhibit the density of states for stacks with TIPS-pentacene, with interlayers in Fig. 2(g) DT (t-DT), Fig. 2(h) NOTP (t-NOTP), and Fig. 2(i) PFDT (t-PFDT), corresponding to the highest, medium, and lowest R_C for the respective OFETs. The energy-level diagrams for the remaining stacks with TIPS-pentacene are displayed in Fig. S4 of the SM. In all plots, the magenta lines mark the molecular orbitals on OSC at the corresponding energy level given on the *y*-axis, and similarly, the cyan lines mark the states on IFE. The highest-occupied molecular orbital (HOMO) and lowest-unoccupied molecular orbital (LUMO) of OSC are marked by blue lines. For IFE, energy bands of the Au slab are modified from the

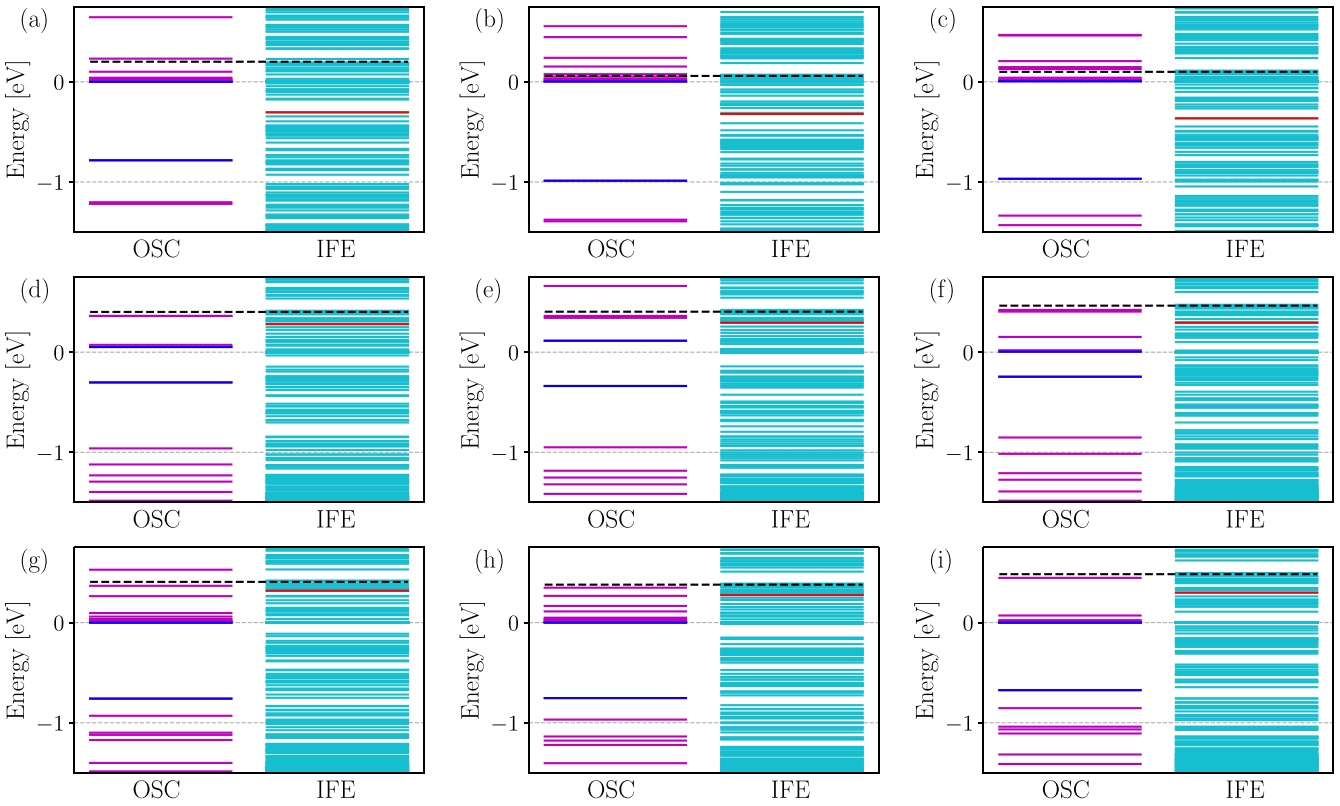

FIG. 2. Energy level diagram of OSC-IFE interfaces for (a) *n*-PFDT, (b) *n*-CT, (c) *n*-MeTP, (d) f-MeOTP, (e) f-ATP, (f) f-PFOT, (g) t-DT, (h) t-NOTP, and (i) t-PFDT. Magenta lines represent the energy levels of orbitals of OSC, while cyan lines are the states of IFE. Blue lines mark the HOMO and LUMO orbitals, while red lines the VBM for systems with *n*-type OSC in (a)–(c) and CBM for systems with *p*-type OSC in (d)–(i). The black dotted lines represent the Fermi level.

pristine slab due to functionalization with the SAM molecule. A red line marks the conduction band minimum (CBM) of IFE in stacks with *p*-type OSCs or a valance band maximum (VBM) of IFE in stacks with *n*-type OSC. The black dotted lines represent the Fermi level for the stack.

Charge injection involves the transfer of electrons from occupied states of IFE to LUMO of OSC in the case of N1400. In contrast, hole injection to TFB or TIPS-pentacene involves the transfer of electrons from the HOMO of OSC to unoccupied states in IFE. For stacks with N1400, VBM represents the energy level below which states are occupied, from where electrons may be injected. The energy difference (ΔE) between occupied states and LUMO acts as an energy barrier that must be overcome for electron injection; the minimum is between the VBM of IFE and the LUMO of OSC. It is apparent that the energy-level alignment depends on the interlayer present at the interface. The interlayer modulates the energy level and generates realignment during interface formation based on the molecular interactions between IFE and OSC molecules driven by the microscopic interactions at the interface. The IFE-OSC system with low ΔE tends to favor charge transfer. ΔE between VBM and LUMO of N1400 is 0.31 eV for *n*-PFDT, while it is 0.32 eV for *n*-CT, and is 0.37 eV for *n*-MeTP. For TFB and TIPS-pentacene, all states above CBM are partially occupied or unoccupied, to where electrons from the HOMO of the OSC may be transferred. Hence ΔE between the HOMO of OSC and the unoccupied states of IFE acts as an energy barrier that must be overcome for hole injection, the minimum of which is between the HOMO of OSC and the CBM of IFE. For stacks with TFB, ΔE for *f*-MeOTP is 0.58 eV while it is 0.64 eV for *f*-ATP, and 0.53 eV for *f*-PFOT. For TIPS-pentacene stacks, ΔE is 1.08 eV for *t*-DT, 1.03 eV for *t*-NOTP, and 0.97 eV for *t*-PFDT.

For stacks with either OSC, as ΔE acts as an energy barrier for the injection of charge, a lower value of ΔE indicates a higher feasibility of electron transfer across the interface. Therefore, the reduction in R_C of a device is expected to be the greatest for the interlayer, leading to the lowest ΔE between relevant states at the interface. However, the values of ΔE are not entirely correlated with device R_C for stacks with any OSCs. The value of minimum ΔE for stacks with *n*-MeTP is higher than that of *n*-CT despite the R_C of the corresponding OFET with *n*-MeTP being lower. Similarly, the minimum ΔE of *f*-ATP is higher than that of *f*-MeOTP despite the R_C of the corresponding OFET with the *f*-ATP being lower. This indicates that the presence of interlayer modulates the energy levels at the interface; however, ΔE does not solely determine the interfacial resistance. Hence, other factors must be taken into account to evaluate the effectiveness of interlayer.

As charge transfer involves states of IFE and orbitals of OSC, the extent of interactions among them determine the charge transfer aside from respective energy levels. Accordingly, the charge transfer integral between all states of IFE with relevant frontier orbitals of OSC was calculated. Charge transfer integral is a measure of the strength of electronic coupling and, hence, of the feasibility of charge transfer between the participating entities. J is the charge transfer integral calculated for the orbital of the OSC molecule with states of the microscopic slice of the interface, thus representing the increased electronic coupling brought about by the interlayer molecule. It was shown previously that the presence of interlayers affects the delocalization of orbitals and interface, and hence, the extent of overlap possible between participating entities. J measures the effect of this on charge transfer. Figure 3 shows charge transfer integral values between frontier orbitals of OSC and states on IFE. For all plots, the *x*-axis contains the ΔE between states on respective IFE, and either LUMO of N1400 or HOMO of TIPS-pentacene or TFB, while the *y*-axis contains the corresponding log of values of average charge transfer integral (J_E) between all states at that energy level and the frontier orbital of OSC. Figures 3(a) to 3(c) show the electronic coupling between states on IFE having PFDT, CT, or MeTP molecules, respectively, and LUMO of N1400. J_E between LUMO of N1400 and the VBM of IFE is 2.89×10^{-7} eV for *n*-PFDT, while it is 5.82×10^{-5} eV for *n*-CT, and it is 5.03×10^{-5} eV for *n*-MeTP. Similarly, Figures 3(d) to 3(f) show the electronic coupling between states on IFE having MeOTP, ATP, or PFOT molecules, respectively, and HOMO of TFB. The value of J_E between CBM of IFE and HOMO of TFB is 1.20×10^{-4} eV for *f*-MeOTP, while it is 1.06×10^{-3} eV for *f*-ATP, and it is 2.29×10^{-3} eV for *f*-PFOT. Further, Figs. 3(g) to 3(i) show the electronic coupling between states on IFE having DT, NOTP, or PFDT molecules, respectively, and HOMO of TIPS-pentacene. The value of J_E between CBM of IFE and HOMO of TIPS-pentacene is 7.94×10^{-5} eV for *t*-DT, while it is 9.90×10^{-5} eV for *t*-NOTP and it is 3.40×10^{-7} eV for *t*-PFDT. J_E for remaining OSC-IFE interfaces are displayed in Figs. S5, S6, and S7 of the SM.

In some cases, the trends in ΔE are offset by those of J_E. While ΔE between LUMO of N1400 and VBM of IFE for *n*-PFDT was slightly lower than that of *n*-MeTP, J_E for *n*-PFDT is significantly lower, which indicates low feasibility of the electron injection from VBM of *n*-PFDT to LUMO of N1400. This low feasibility is reflected in the correspondingly measured R_C, which is higher for OFET with *n*-PFDT than with *n*-MeTP. Similarly, while ΔE between HOMO of TFB and CBM of IFE is slightly lower for *f*-MeOTP than for *f*-ATP, J_E for *f*-MeOTP is significantly lower. Therefore, consolidating values of J_E along with ΔE leads to a better understanding of the effect of the interlayer in reducing R_C. However, trends in J_E do not entirely correspond to measured R_C for all cases. J_E is significantly lower for *t*-PFDT than *t*-DT, while the R_C of the OFET with *t*-PFDT is lower than with *t*-DT. This is because states at other energy levels may participate in charge injection. It is apparent from Fig. 3 that for any given IFE-OSC system, states with similar ΔE may have vastly different values of J_E. In such a case, a large J_E may allow charge transfer to or from a state with a slightly higher ΔE to be highly feasible and increase the overall charge injection capacity of the given IFE. Hence, the combined ΔE and J_E for frontier orbitals of the OSC and all relevant IFE states must be accounted for to predict the device R_C.

IV. DISCUSSION

ΔE and J vary with IFE-OSC combinations according to the modulation of interface properties brought about by the interlayer. These parameters represent the reduction in energy barrier and enhancement of electronic coupling at the

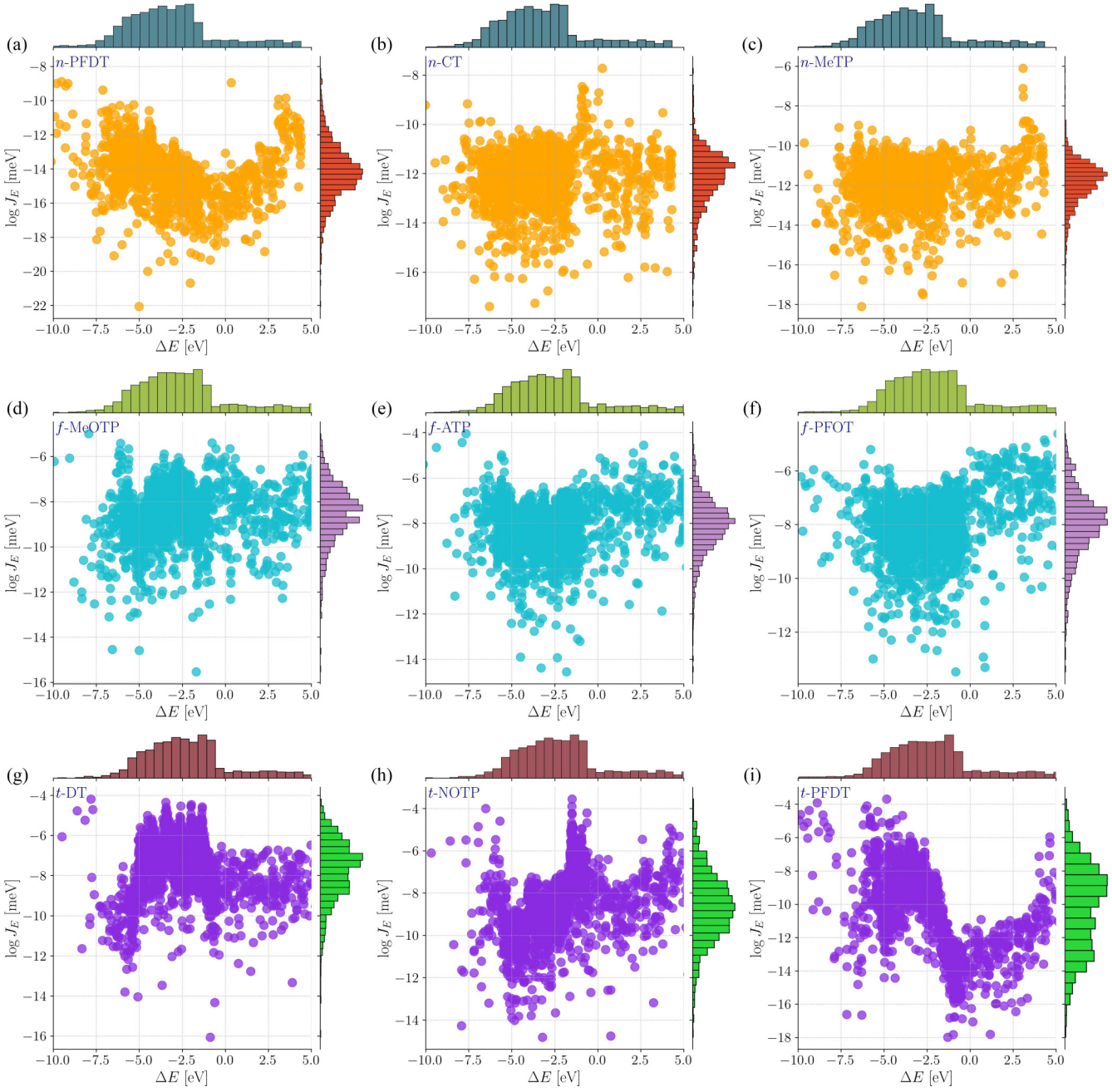

FIG. 3. Charge transfer integral values between LUMO of N1400 or HOMO of TIPS-pentacene or TFB with occupied or unoccupied states of IFE for (a) *n*-PFDT, (b) *n*-CT, (c) *n*-MeTP, (d) *f*-MeOTP, (e) *f*-ATP, (f) *f*-PFOT, (g) *t*-DT, (h) *t*-NOTP, and (i) *t*-PFDT. Plotted on *x*-axis is the difference in energy between the state and orbital, with the log of charge transfer integral between them on *y*-axis. The corresponding 1D histogram for each quantity is shown on the axes.

interface, which would increase the feasibility of charge transfer. However, individually, these parameters do not correlate with device resistance. These parameters cannot be considered individually, as they combine to determine the charge transfer in complex ways. Combining these factors into a function that includes their effects for all participating states enables the calculation of a parameter that correlates directly with device characteristics. Therefore, a function that encompasses both ΔE and J_E and evaluates multiple participating states will be able to predict the reduction in R_C brought about by the interlayer.

For this purpose, the rate of charge injection is calculated for all IFE-OSC systems. The charge transfer rate (k_{ET}) between a system with multiple states and a localized orbital depends on J_E and ΔE as per the Marcus-Hush equation given in Eq. (1) [36,37]

$$k_{ET} = \frac{2\pi}{\hbar}\int J_E^2(E)\frac{1}{1+\exp\frac{E-E_F}{kT}}n(E)\frac{1}{\sqrt{4\pi\lambda kT}} \times \exp\frac{-(\lambda-\Delta E+q\eta)^2}{4\lambda kT}dE. \quad (1)$$

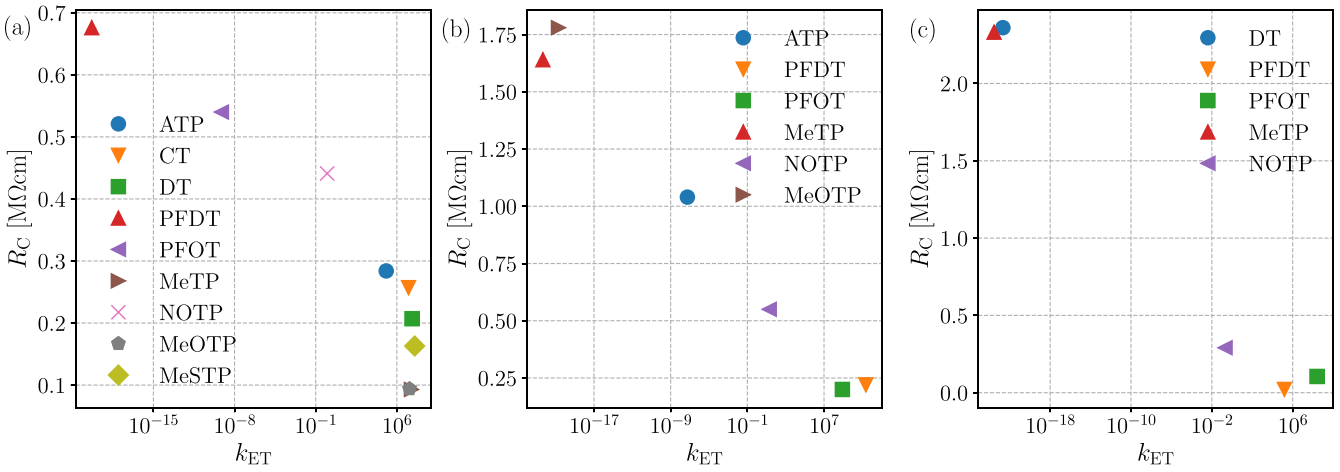

FIG. 4. k_{ET} calculated from parameters obtained by first principles, correlated with measured R_C of devices with (a) N1400, (b) TFB, and (c) TIPS-pentacene as OSC.

Here, E refers to the energy level with n available states on IFE, E_F is the Fermi level of the system, and ΔE is the energy difference between states on IFE with respect to the relevant frontier orbital on OSC. λ is the reorganization energy of the OSC molecule, and η is the overpotential. λ is found to be 0.06 eV for N1400, 0.16 eV for TFB, and 0.13 eV for TIPS-pentacene. The function is integrated over all occupied states, which may transfer an electron to the LUMO of N1400 for n-stacks, or all unoccupied states, which may extract an electron from the HOMO of TFB or TIPS-pentacene for the p- or t- stacks. In the case of states with high ΔE or low J_E, the value of the functions computes to be low and adds less to the final value of k_{ET}. As the dependence on ΔE takes the form of an exponential, states in bands beyond the conduction (valence) band have insignificant function values. For states with similar values of ΔE, the values of J_E determine the value of the function. Notably, our protocol involves uniform first-principles computations for all stacks. No material-specific parameters were specified for the different interfaces. The computational methods were constant for all cases. Computing the parameters representing the interface properties governing charge transport will always correlate with any contact resistance beyond all the systems demonstrated here. The physical processes that were simulated were constant for all cases, and their combined effect was shown to be crucial to charge transport at the interfaces. Figure 4 shows k_{ET} for all IFE-OSC systems correlated with the R_C measured for the respective device. The device R_C decreases with increasing value of k_{ET}, and its dependence on k_{ET} is apparent.

Here, we find that k_{ET} correlates with R_C of devices with modified electrodes. This is attributed to the completeness of the microscopic phenomenon covered in the calculation of k_{ET}. ΔE and J_E are the key parameters that determine the charge transfer process for any contact interface. In the case of functionalized organic-inorganic interfaces, the Marcus-Hush equation provides a function of ΔE and J_E that yields the rate and, accordingly, evaluates the effectiveness of the interlayer. Regardless of the trends in individual parameters J_E, ΔE, or n, trends in k_{ET} are in accordance with measured R_C. k_{ET} is higher for f-PFDT as compared with f-MeOTP due to lower values of ΔE. k_{ET} for t-DT is lower than t-PFOT, similarly, k_{ET} for n-PFDT is lower than for n-MeTP. In both these cases, while the values of ΔE for both systems under comparison are similar, the values of J_E and n are markedly higher for t-PFOT as well as n-MeTP. In this way, the microscopic processes simulated here determine the contact resistance when combined in the form of the given function for k_{ET}. We find that the correlation between k_{ET} and R_C holds for all OSC regardless of its polarity or nature as a small molecule or polymer. Hence, k_{ET} is justified as a universal parameter to predict the extent of reduction of R_C by the interlayer. k_{ET} correlates strongly with the measured resistance at the interface in the form of R_C as the resistance to the charge transfer emerges from the microscopic interactions at the interface; these effects are measured in formulating k_{ET}. Further, we note that the mobility of the devices reported in Ref. [35] are also well correlated with k_{ET}, as shown in Fig. S8. This further indicates k_{ET} to be a suitable parameter for evaluating the interlayer for an organic device. Calculated rates for all systems and measured contact resistance and mobility values for all devices are given in Table S1 of the SM. Therefore, the values of k_{ET} can predict the extent of the reduction in R_C brought about by the interlayer at the given interface and the resulting device performance. Hence, calculating k_{ET} by the Marcus-Hush equation based on quantities obtained from first principles establishes a protocol for predicting the contact resistance for a given interface.

V. CONCLUSION

DFT-based computations were performed on stacks representing contact interfaces of organic devices with functionalized electrodes to simulate the process of charge injection. Calculations according to the POD method led to values of parameters governing charge transfer from (to) occupied (unoccupied) states on IFE to (from) LUMO (HOMO) of OSC. It was shown that the energy difference between states participating in charge transfer and the electronic coupling between them are crucial parameters governing the charge

transfer process at the interface. It was found that trends in ΔE and J_E were not sufficiently correlated with device properties individually. However, the charge transfer rate, a function of ΔE and J_E, correlates well with the R_C of devices with functionalized electrodes for each OSC. k_{ET} captures the various physical effects at the interface that determine charge injection and, consequently, the contact resistance. k_{ET} can be calculated from the first principles for any contact interface, as demonstrated here for variations in OSC and IFE. In all cases, the correlation between R_C and k_{ET} holds. Therefore, k_{ET} is a universal parameter correlating microscopic phenomenon with device behavior.

ACKNOWLEDGMENTS

The authors gratefully acknowledge the Indian Institute of Technology Gandhinagar, India, for providing research facilities and support. A.M. acknowledges the SERB (Grant No. SRG/2022/001532) project for funding. K.P. and A.M. thank PARAM Ananta for computational resources.

[1] C.-A. Di, F. Zhang, and D. Zhu, Multi-functional integration of organic field-effect transistors (OFETs): Advances and perspectives, Adv. Mater. **25**, 313 (2013).

[2] B. Geffroy, P. Le Roy, and C. Prat, Organic light-emitting diode (OLED) technology: Materials, devices and display technologies, Polym. Int. **55**, 572 (2006).

[3] C. J. Brabec, A. Distler, X. Du, H.-J. Egelhaaf, J. Hauch, T. Heumueller, and N. Li, Material strategies to accelerate OPV technology toward a GW technology, Adv. Energy Mater. **10**, 2001864 (2020).

[4] S. K. Park, J. E. Anthony, and T. N. Jackson, Solution-processed tips-pentacene organic thin-film-transistor circuits, IEEE Electron Device Lett. **28**, 877 (2007).

[5] W. Wu, Z. Chen, Y. Zhan, B. Liu, W. Song, Y. Guo, J. Yan, X. Yang, Z. Zhou, and W.-Y. Wong, An efficient hole transporting polymer for quantum dot light-emitting diodes, Adv. Mater. Interfaces **8**, 2100731 (2021).

[6] G. Casula, S. Lai, L. Matino, F. Santoro, A. Bonfiglio, and P. Cosseddu, Printed, low-voltage, all-organic transistors and complementary circuits on paper substrate, Adv. Electron. Mater. **6**, 1901027 (2020).

[7] J. C. Scott and G. G. Malliaras, Charge injection and recombination at the metal–organic interface, Chem. Phys. Lett. **299**, 115 (1999).

[8] Y. Xu, H. Sun, and Y.-Y. Noh, Schottky barrier in organic transistors, IEEE Trans. Electron Devices **64**, 1932 (2017).

[9] F. Amy, C. Chan, and A. Kahn, Polarization at the gold/pentacene interface, Org. Electron. **6**, 85 (2005).

[10] N. Koch, A. Kahn, J. Ghijsen, J.-J. Pireaux, J. Schwartz, R. L. Johnson, and A. Elschner, Conjugated organic molecules on metal versus polymer electrodes: Demonstration of a key energy level alignment mechanism, Appl. Phys. Lett. **82**, 70 (2003).

[11] D. Natali and M. Caironi, Charge injection in solution-processed organic field-effect transistors: Physics, models and characterization methods, Adv. Mater. **24**, 1357 (2012).

[12] H. Vázquez, W. Gao, F. Flores, and A. Kahn, Energy level alignment at organic heterojunctions: Role of the charge neutrality level, Phys. Rev. B **71**, 041306(R) (2005).

[13] M. Waldrip, O. D. Jurchescu, D. J. Gundlach, and E. G. Bittle, Contact resistance in organic field-effect transistors: Conquering the barrier, Adv. Funct. Mater. **30**, 1904576 (2020).

[14] J. Frisch, H. Glowatzki, S. Janietz, and N. Koch, Solution-based metal electrode modification for improved charge injection in polymer field-effect transistors, Org. Electron. **10**, 1459 (2009).

[15] F. Huang, H. Liu, X. Li, and S. Wang, Highly efficient hole injection/transport layer-free oleds based on self-assembled monolayer modified ito by solution-process, Nano Energy **78**, 105399 (2020).

[16] Y. Lin, Y. Zhang, J. Zhang, M. Marcinskas, T. Malinauskas, A. Magomedov, M. I. Nugraha, D. Kaltsas, D. R. Naphade, G. T. Harrison *et al.*, 18.9% efficient organic solar cells based on n-doped bulk-heterojunction and halogen-substituted self-assembled monolayers as hole extracting interlayers, Adv. Energy Mater. **12**, 2202503 (2022).

[17] I. H. Campbell, S. Rubin, T. A. Zawodzinski, J. D. Kress, R. L. Martin, D. L. Smith, N. N. Barashkov, and J. P. Ferraris, Controlling Schottky energy barriers in organic electronic devices using self-assembled monolayers, Phys. Rev. B **54**, R14321 (1996).

[18] J. Kim, A. Gulans, and C. Draxl, Work-function modification of PEG(thiol) adsorbed on the Au(111) surface: A first-principles study, Phys. Rev. Mater. **4**, 116001 (2020).

[19] C. Liu, Y. Xu, and Y.-Y. Noh, Contact engineering in organic field-effect transistors, Mater. Today **18**, 79 (2015).

[20] H. Ishii, K. Sugiyama, E. Ito, and K. Seki, Energy level alignment and interfacial electronic structures at organic/metal and organic/organic interfaces, Adv. Mater. **11**, 605 (1999).

[21] O. T. Hofmann, D. A. Egger, and E. Zojer, Work-function modification beyond pinning: When do molecular dipoles count? Nano Lett. **10**, 4369 (2010).

[22] N. B. Kotadiya, H. Lu, A. Mondal, Y. Ie, D. Andrienko, P. W. Blom, and G.-J. A. Wetzelaer, Universal strategy for ohmic hole injection into organic semiconductors with high ionization energies, Nat. Mater. **17**, 329 (2018).

[23] M. T. Greiner, M. G. Helander, W.-M. Tang, Z.-B. Wang, J. Qiu, and Z.-H. Lu, Universal energy-level alignment of molecules on metal oxides, Nat. Mater. **11**, 76 (2012).

[24] G. Heimel, L. Romaner, E. Zojer, and J.-L. Bredas, The interface energetics of self-assembled monolayers on metals, Acc. Chem. Res. **41**, 721 (2008).

[25] G. Heimel, L. Romaner, E. Zojer, and J.-L. Brédas, Toward control of the metal-organic interfacial electronic structure in molecular electronics: A first-principles study on self-assembled monolayers of π-conjugated molecules on noble metals, Nano Lett. **7**, 932 (2007).

[26] I. Katsouras, V. Geskin, A. J. Kronemeijer, P. W. Blom, and D. M. de Leeuw, Binary self-assembled monolayers: Apparent exponential dependence of resistance on average molecular length, Org. Electron. **12**, 857 (2011).

[27] C. George III, H. Yoshida, W. A. Goddard III, S. S. Jang, and Y.-H. Kim, Charge transport through polyene self-assembled monolayers from multiscale computer simulations, J. Phys. Chem. B **112**, 14888 (2008).

[28] K. Patrikar, U. Bothra, V. R. Rao, and D. Kabra, Charge carrier doping as mechanism of self-assembled monolayers functionalized electrodes in organic field effect transistors, Adv. Mater. Interfaces **9**, 2101377 (2022).

[29] G. Heimel, L. Romaner, J.-L. Brédas, and E. Zojer, Odd- even effects in self-assembled monolayers of ω-(Biphenyl-4-yl) alkanethiols: A first-principles study, Langmuir **24**, 474 (2008).

[30] K. Patrikar and A. Mondal, Polarity and orbital driven reduction in contact resistance in organic devices with functionalized electrodes, J. Chem. Phys. **159**, 121102 (2023).

[31] N. Ferri, A. Ambrosetti, and A. Tkatchenko, Electronic charge rearrangement at metal/organic interfaces induced by weak van der Waals interactions, Phys. Rev. Mater. **1**, 026003 (2017).

[32] Z. Futera and J. Blumberger, Electronic couplings for charge transfer across molecule/metal and molecule/semiconductor interfaces: Performance of the projector operator-based diabatization approach, J. Phys. Chem. C **121**, 19677 (2017).

[33] I. Kondov, M. Čížek, C. Benesch, H. Wang, and M. Thoss, Quantum dynamics of photoinduced electron-transfer reactions in dye-semiconductor systems: First-principles description and application to coumarin 343-TiO_2, J. Phys. Chem. C **111**, 11970 (2007).

[34] K. Patrikar, V. R. Rao, D. Kabra, and A. Mondal, Understanding the microscopic origin of the contact resistance at the polymer–electrode interface, ACS Appl. Mater. Interfaces **15**, 49427 (2023).

[35] D. Boudinet, M. Benwadih, Y. Qi, S. Altazin, J.-M. Verilhac, M. Kroger, C. Serbutoviez, R. Gwoziecki, R. Coppard, G. Le Blevennec *et al.*, Modification of gold source and drain electrodes by self-assembled monolayer in staggered n-and p-channel organic thin film transistors, Org. Electron. **11**, 227 (2010).

[36] R. A. Marcus, On the theory of electron-transfer reactions. VI. Unified treatment for homogeneous and electrode reactions, J. Chem. Phys. **43**, 679 (1965).

[37] N. S. Hush, Adiabatic rate processes at electrodes. I. Energy-charge relationships, J. Chem. Phys. **28**, 962 (1958).

[38] P. Hohenberg and W. Kohn, Inhomogeneous electron gas, Phys. Rev. **136**, B864 (1964).

[39] W. Kohn and L. J. Sham, Self-consistent equations including exchange and correlation effects, Phys. Rev. **140**, A1133 (1965).

[40] J. Hutter, M. Iannuzzi, F. Schiffmann, and J. VandeVondele, CP2K: Atomistic simulations of condensed matter systems, WIREs Comput. Mol. Sci. **4**, 15 (2014).

[41] J. VandeVondele, M. Krack, F. Mohamed, M. Parrinello, T. Chassaing, and J. Hutter, Quickstep: Fast and accurate density functional calculations using a mixed Gaussian and plane waves approach, Comput. Phys. Commun. **167**, 103 (2005).

[42] J. P. Perdew, K. Burke, and M. Ernzerhof, Generalized gradient approximation made simple, Phys. Rev. Lett. **77**, 3865 (1996).

[43] C. Hartwigsen, S. Gœdecker, and J. Hutter, Relativistic separable dual-space Gaussian pseudopotentials from H to Rn, Phys. Rev. B **58**, 3641 (1998).

[44] S. Goedecker, M. Teter, and J. Hutter, Separable dual-space Gaussian pseudopotentials, Phys. Rev. B **54**, 1703 (1996).

[45] A. Schäfer, C. Huber, and R. Ahlrichs, Fully optimized contracted Gaussian basis sets of triple zeta valence quality for atoms Li to Kr, J. Chem. Phys. **100**, 5829 (1994).

[46] F. Weigend and R. Ahlrichs, Balanced basis sets of split valence, triple zeta valence and quadruple zeta valence quality for h to rn: Design and assessment of accuracy, Phys. Chem. Chem. Phys. **7**, 3297 (2005).

[47] Y. A. Berlin, G. R. Hutchison, P. Rempala, M. A. Ratner, and J. Michl, Charge hopping in molecular wires as a sequence of electron-transfer reactions, J. Phys. Chem. A **107**, 3970 (2003).

[48] M. J. Frisch, G. W. Trucks, H. B. Schlegel, G. E. Scuseria, M. A. Robb, J. R. Cheeseman, G. Scalmani, V. Barone, G. A. Petersson, H. Nakatsuji, X. Li, M. Caricato, A. Marenich, J. Bloino, B. G. Janesko, R. Gomperts, B. Mennucci, H. P. Hratchian, J. V. Ortiz, A. F. Izmaylov *et al.*, Gaussian 09, Revision A.02, Gaussian, Inc., Wallingford CT, 2016.

[49] A. D. Becke, A new inhomogeneity parameter in density-functional theory, J. Chem. Phys. **109**, 2092 (1998).

[50] C. Lee, W. Yang, and R. G. Parr, Development of the Colle-Salvetti correlation-energy formula into a functional of the electron density, Phys. Rev. B **37**, 785 (1988).

[51] J. P. Perdew, Density-functional approximation for the correlation energy of the inhomogeneous electron gas, Phys. Rev. B **33**, 8822 (1986).

[52] R. Ditchfield, W. J. Hehre, and J. A. Pople, Self-consistent molecular-orbital methods. IX. An extended Gaussian-type basis for molecular-orbital studies of organic molecules, J. Chem. Phys. **54**, 724 (1971).

[53] G. A. Petersson, A. Bennett, T. G. Tensfeldt, M. A. Al-Laham, W. A. Shirley, and J. Mantzaris, A complete basis set model chemistry. I. The total energies of closed-shell atoms and hydrides of the first-row elements, J. Chem. Phys. **89**, 2193 (1988).

[54] See Supplemental Material at http://link.aps.org/supplemental/10.1103/PhysRevMaterials.8.054606 for the schematic of computational setup, the density of states, charge transfer integrals, mobility versus rates, and tabulated values.